Journal of Power Sources 265 (2014) 118–124

Contents lists available at ScienceDirect

Journal of Power Sources

journal homepage: www.elsevier.com/locate/jpowsour

Short communication

Submicron lithium nickel manganese oxide spinel with long cycling stability and high rate performance prepared by a facile route

Guoqing Wang [a,b], Jian Xie [a,b,*], Chunyang Wu [a], Shichao Zhang [c], Gaoshao Cao [b], Xinbing Zhao [a,b]

[a] State Key Laboratory of Silicon Materials, Department of Materials Science and Engineering, Zhejiang University, Hangzhou 310027, China
[b] Key Laboratory of Advanced Materials and Applications for Batteries of Zhejiang Province, China
[c] School of Materials Science and Engineering, Beijing University of Aeronautics and Astronautics, Beijing 100191, China

HIGHLIGHTS

- We synthesize submicron $LiNi_{0.5}Mn_{1.5}O_4$ by a facile route.
- $LiNi_{0.5}Mn_{1.5}O_4$ shows excellent rate performance and cycling stability.
- $LiNi_{0.5}Mn_{1.5}O_4$–MCMB cells show promising high-energy-density applications.

GRAPHICAL ABSTRACT

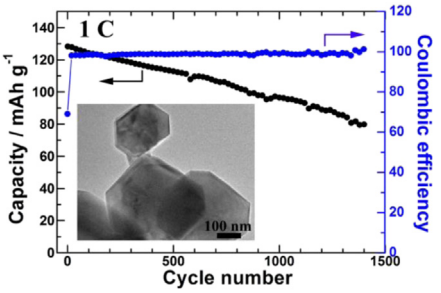

ARTICLE INFO

Article history:
Received 22 February 2014
Received in revised form
19 April 2014
Accepted 27 April 2014
Available online 9 May 2014

Keywords:
Lithium nickel manganese oxide
High-voltage cathode
Submicron size
Electrochemical performance
Full cell

ABSTRACT

Lithium nickel manganese oxide ($LiNi_{0.5}Mn_{1.5}O_4$) shows promising applications in next-generation Li-ion batteries due to its high working voltage. In this work, submicron $LiNi_{0.5}Mn_{1.5}O_4$ has been synthesized by a facile solid-phase route and its electrochemical performance has been investigated in both half cells and full cells using mesocarbon microbeads as anodes. In $LiNi_{0.5}Mn_{1.5}O_4$–Li cells, $LiNi_{0.5}Mn_{1.5}O_4$ shows excellent rate performance and high-rate cycling stability. At 20 C, $LiNi_{0.5}Mn_{1.5}O_4$ can yield a discharge capacity of 105.8 mAh g^{-1}. After 1400 cycles at 1 C, a discharge capacity of around 80 mAh g^{-1} can be still delivered. The $LiNi_{0.5}Mn_{1.5}O_4$-limited full cells exhibit a working voltage of around 4.5 V and a discharge capacity of 90.0 mAh g^{-1} after 120 cycles at 1 C. The excellent electrochemical performance of $LiNi_{0.5}Mn_{1.5}O_4$ can be attributed to a combination of submicron size, durability of Mn^{3+} at high rates and small-size induced protective film.

© 2014 Elsevier B.V. All rights reserved.

1. Introduction

Li-ion batteries currently show promising applications as power sources for electric vehicles (EVs) and hybrid electric vehicles (HEVs). Cathode materials with high specific capacity, enhanced rate performance, long cycle life, low cost, and high safety have been intensively investigated recently to meet the stringent requirements for EVs and HEVs applications [1–4]. Although spinel $LiMn_2O_4$ and olivine $LiFePO_4$ are of broad interest because of their

* Corresponding author. State Key Laboratory of Silicon Materials, Department of Materials Science and Engineering, Zhejiang University, Hangzhou 310027, China. Tel.: +86 571 87952181; fax: +86 571 87951451.
E-mail address: xiejian1977@zju.edu.cn (J. Xie).

http://dx.doi.org/10.1016/j.jpowsour.2014.04.125
0378-7753/© 2014 Elsevier B.V. All rights reserved.

resource abundance, environmental friendliness, and high safety [5], they exhibit low energy density for either low working voltage or low specific capacity. Using high-voltage cathode is one of the practical strategies to increase the energy density of Li-ion batteries [6–8]. Among various candidates, spinel $LiNi_{0.5}Mn_{1.5}O_4$ has received a special attention because of its low cost and high working voltage of around 4.7 V [9–20]. For EVs and HEVs applications, good rate performance and high-rate cycling stability are also indispensable in addition to high working voltage.

Using materials with a small size, for example nanomaterials, provides a practical solution to this issue since small-sized materials have short Li-ion diffusion pathways and large contact area with electrolyte. Previous work has shown that $LiNi_{0.5}Mn_{1.5}O_4$ with various nanostructures, such as nanoparticles [12,21–24], nanoflakes [25], nanorods/nanowires [26–28], and hollow spheres [29], could demonstrate enhanced rate capability and high-rate cycling stability. Chen et al. [25] reported surface oriented, nanoflake-stacked $LiNi_{0.5}Mn_{1.5}O_4$ that can yield a discharge capacity as high as 96 mAh g^{-1} at 50 C. High capacity retention of 86% can be achieved after 500 cycles at 1 C for this material. Porous $LiNi_{0.5}Mn_{1.5}O_4$ nanorods reported by Zhang et al. [28] could exhibit excellent high-rate cycling stability with 91% of the initial capacity maintained after 500 cycles at 5 C. However, the synthesis of these nanostructures generally involves a relatively complex solution route, where surfactants or templates are always necessary. For example, triblock copolymer F127 was used as the template to obtain the desired surface orientation of $LiNi_{0.5}Mn_{1.5}O_4$ [25].

In this work, we report a facile solid-phase route to synthesize submicron $LiNi_{0.5}Mn_{1.5}O_4$ with excellent electrochemical performance in both half and full cells. The submicron structure allows rapid Li-ion transport both at particle/electrolyte interface and in bulk particle. The submicron structure also promotes the formation of an effective surface film to inhibit Mn and Ni dissolution. The protective effect of the surface film also makes Mn^{3+} survive long-term cycling at high rates, which is critical for high-rate cycling stability of $LiNi_{0.5}Mn_{1.5}O_4$. The excellent electrochemical performance of submicron $LiNi_{0.5}Mn_{1.5}O_4$ as well as its easy synthesis route makes it possible for large-scale applications in EVs and HEVs.

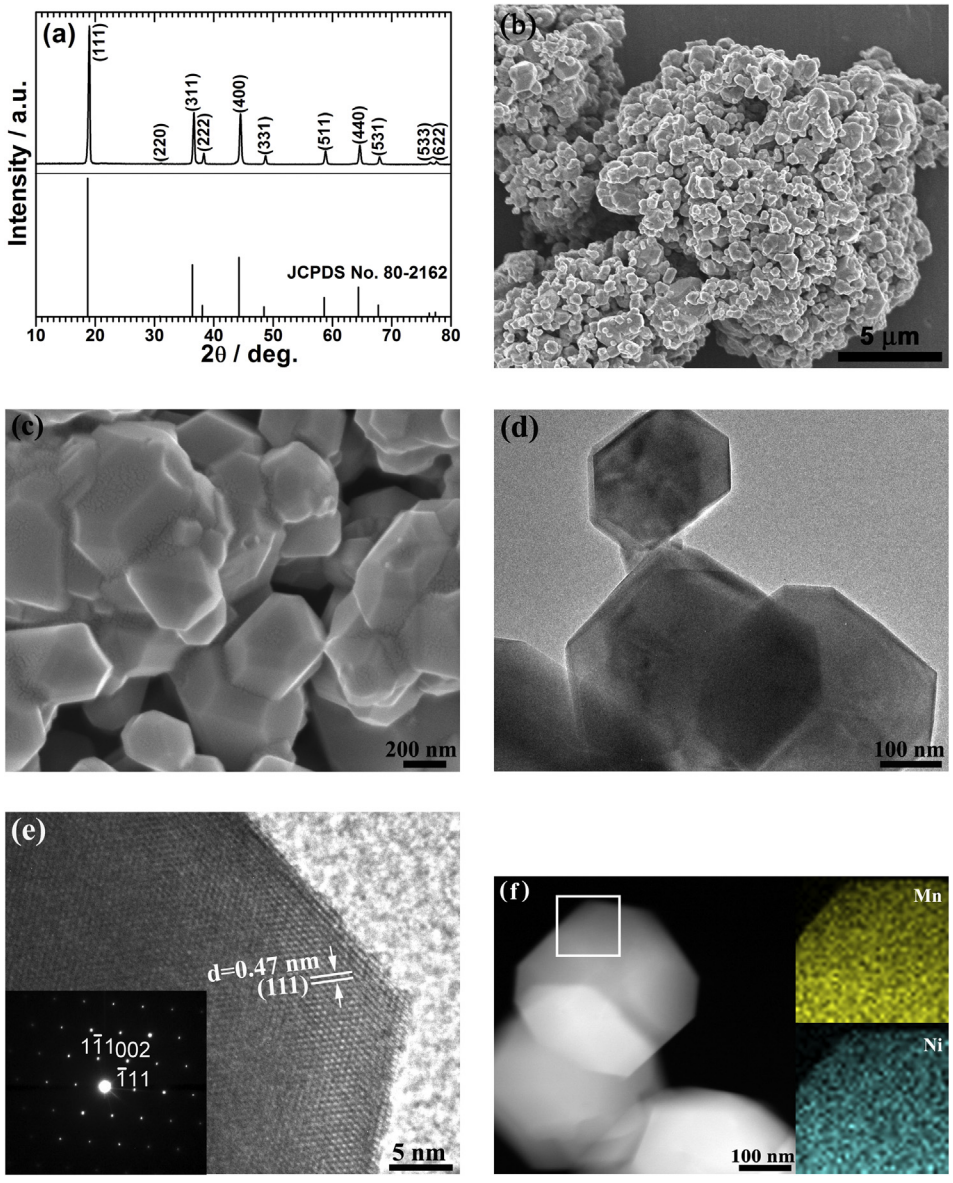

Fig. 1. (a) XRD patterns, (b, c) SEM images, (d) TEM image, (e) HRTEM image and SAED patterns, and (f) EDS mapping of submicron $LiNi_{0.5}Mn_{1.5}O_4$.

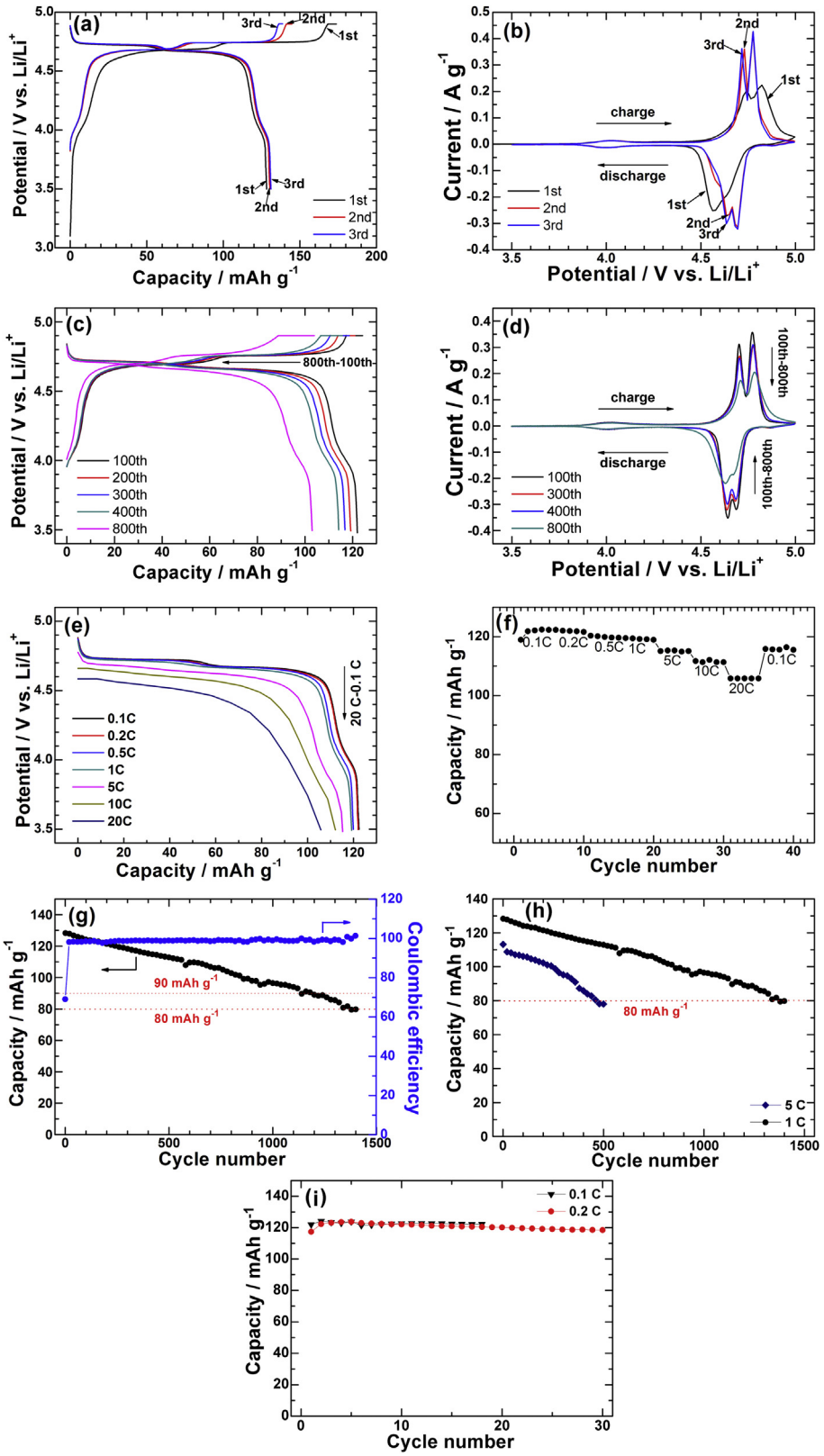

Fig. 2. Electrochemical performance of submicron $LiNi_{0.5}Mn_{1.5}O_4$ in half cells: (a) the first three voltage profiles at 0.1 C, (b) the first three CV scans at 0.1 mV s^{-1}, (c) voltage profiles on the 100–800th cycles at 1 C, (d) CV scans on the 100–800th cycles at 0.1 mV s^{-1}, (e) discharge curves at various rates, (f) rate dependence of discharge capacity, (g) cycling stability and coulombic efficiency at 1 C, (h) cycling stability at 1 C and 5 C, and (i) cycling stability at 0.1 C and 0.2 C.

2. Experimental

2.1. Preparation and characterization of $LiNi_{0.5}Mn_{1.5}O_4$

$LiNi_{0.5}Mn_{1.5}O_4$ was prepared by a facile solid-phase route using stoichiometric amounts of MnO_2, NiO and Li_2CO_3 (5% excess) as the precursors. The precursors were thoroughly mixed by shock-type ball milling at 20 Hz for 1 h. The mixed precursors were placed in the center of a tubular furnace with the temperature increased to 800 °C at 2 °C per minute in air. After firing at this temperature for 20 h, the furnace was cooled to room temperature at 1 °C min^{-1} to obtain the final product. The phases in the product were analyzed by X-ray diffraction (XRD) on a Rigaku D/Max-2550pc powder diffractometer equipped with Cu K_α radiation ($\lambda = 0.1542$ nm). The morphology of the product was observed by field-emission scanning electron microscopy (SEM) on an FEI-sirion microscope, transmission electron microscopy (TEM) and high-resolution TEM (HRTEM) on a JEM 2100F microscope.

2.2. Electrochemical measurements

The electrochemical performance of the product was evaluated by galvanostatic cycling using CR2025-type coin cells. The electrode slurry was made by mixing 75 wt% $LiNi_{0.5}Mn_{1.5}O_4$, 15 wt% acetylene black (AB) and 10 wt% polyvinylidene fluoride (PVDF) and stirring in *N*-methyl pyrrolidone (NMP) for 2 h. The working electrodes were made by spreading the slurry onto Al foils and dried at 100 °C under vacuum for 10 h. The electrodes were then assembled into half cells in an Ar-filled glove box using Li foils as the counter electrodes and Celgard 2300 polypropylene membranes as the separators. The electrolyte was 1 M $LiPF_6$ dissolved in ethylene carbonate (EC)/dimethyl carbonate (DMC) (1:1 in volume). The half cells were charged and discharged at various current densities between 3.5 and 4.9 V vs. Li/Li^+ on a Neware battery tester (Shenzhen, China). Cyclic voltammetry (CV) scanning was performed on an Arbin BT2000 system between 3.5 and 5.0 V vs. Li/Li^+ at 0.1 mV s^{-1}. Coin-type full cells were also assembled in a similar manner using mesocarbon microbeads (MCMB) as the anodes. The $LiNi_{0.5}Mn_{1.5}O_4$–MCMB cells were galvanostatically cycled at 3.4–4.8 V under 0.1 C and 1 C. The full cells are cathode limited and 1 C corresponds to 150 mA g^{-1} for both half and full cells. All of the electrochemical measurements were carried out at room temperature.

3. Results and discussion

Fig. 1a shows the XRD patterns of $LiNi_{0.5}Mn_{1.5}O_4$ prepared at 800 °C in air. The diffraction peaks of the product agree well with the standard patterns of spinel $LiNi_{0.5}Mn_{1.5}O_4$ (JCPDS No. 80-2162) with no obvious impurities. This suggests that the expected impurities such as rock-salt $Li_xNi_{1-x}O$ are at a low content. The spinel can be well indexed to disordered $LiNi_{0.5}Mn_{1.5}O_{4-\delta}$ with space group $Fd\bar{3}m$ rather than ordered $LiNi_{0.5}Mn_{1.5}O_4$ with space group $P4_332$ due to the absence of the superstructure peaks in the patterns. For simplicity, $LiNi_{0.5}Mn_{1.5}O_4$ is still used in the following sections.

The morphology of $LiNi_{0.5}Mn_{1.5}O_4$ was observed by SEM, TEM and HRTEM. SEM image in Fig. 1b shows that the sample is composed of small sized primary particles which aggregate to large sized aggregations of several microns. High-magnification SEM image in Fig. 1c indicates the faceted structure of the primary $LiNi_{0.5}Mn_{1.5}O_4$ particles. SEM image also reveals that the size of the primary $LiNi_{0.5}Mn_{1.5}O_4$ particles is below 500 nm. The small size of $LiNi_{0.5}Mn_{1.5}O_4$ is further confirmed by TEM observation (Fig. 1d). This means that submicron structure of $LiNi_{0.5}Mn_{1.5}O_4$ can be preserved even after high-temperature firing at 800 °C. Fig. 1e gives HRTEM image of $LiNi_{0.5}Mn_{1.5}O_4$. The fringe spacings of 0.47 nm in HRTEM correspond to the interplanar distances of (111) planes of $LiNi_{0.5}Mn_{1.5}O_4$. The single crystalline character of a single primary particle is also revealed by HRTEM and selected area electron diffraction (SAED). Fig. 1f shows the dark-field TEM image and energy dispersive X-ray spectroscopy (EDS) mapping of Mn and Ni elements. The EDS mapping indicates uniform distribution of Mn and Ni. As a result, submicron $LiNi_{0.5}Mn_{1.5}O_4$ has been obtained by this facile preparation method.

Fig. 2a shows the first three voltage profiles of submicron $LiNi_{0.5}Mn_{1.5}O_4$ at 0.1 C (1 C = 150 mA g^{-1}), which exhibit a quasi-plateau at 3.9–4.2 V and two successive plateaus at around 4.7 V. The successive plateaus at around 4.7 V are related to Ni^{2+}/Ni^{3+} and Ni^{3+}/Ni^{4+} redox couples, whereas the quasi-plateau at 3.9–4.2 V originates from the Mn^{3+}/Mn^{4+} redox couple. The appearance of Mn^{3+}/Mn^{4+} couple is in accord with the disordered phase of $LiNi_{0.5}Mn_{1.5}O_{4-\delta}$ (space group $Fd\bar{3}m$) revealed by XRD. The oxygen loss at high temperature is charge compensated by reducing Mn^{4+} to Mn^{3+} with the formation of oxygen deficiency [16,30]. However, the expected formation of rock-salt $Li_yNi_{1-y}O$ phase [9,16,30] accompanied by the oxygen loss is not significant. The first charge and discharge capacities of $LiNi_{0.5}Mn_{1.5}O_4$ are 173.8 and 128.3 mAh g^{-1}, respectively. The low coulombic efficiency in the first cycle is caused by electrolyte oxidation by Ni^{3+}/Ni^{4+} to form a surface film [16]. The small size of $LiNi_{0.5}Mn_{1.5}O_4$ may promote the oxidation reaction by increasing the contact with electrolyte. The charge and discharge capacities are stabilized at 138.7 and 131.1 mAh g^{-1} in the third cycle, with the coulombic efficiency increased to 95%. The high specific capacity is ascribed to low content of $Li_yNi_{1-y}O$ impurity and good crystallization of $LiNi_{0.5}Mn_{1.5}O_4$, while the increased coulombic efficiency is due to

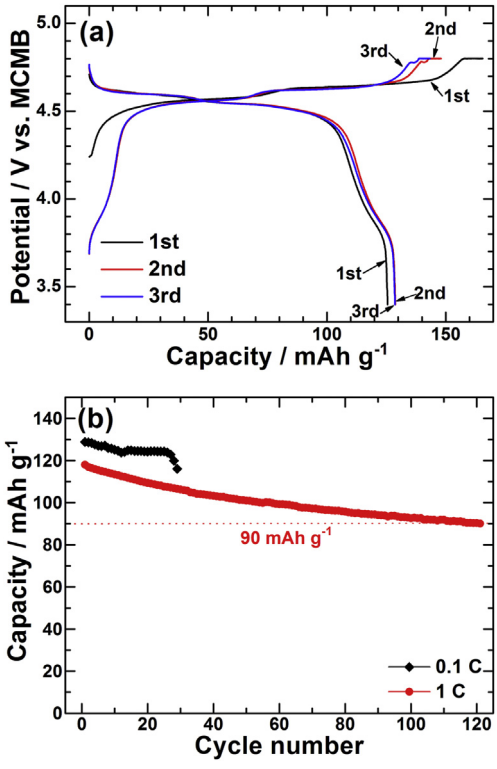

Fig. 3. Electrochemical performance of submicron $LiNi_{0.5}Mn_{1.5}O_4$ in full cells: (a) the first three voltage profiles at 0.1 C, and (b) cycling stability at 0.1 C and 1 C.

effective inhibition of electrolyte oxidation by the surface film in the subsequent cycles. The capacity contributed by Mn^{3+}/Mn^{4+} is estimated to be 8% of the total capacity of $LiNi_{0.5}Mn_{1.5}O_4$ by comparing the plateau length between Mn^{3+}/Mn^{4+} and Ni^{2+}/Ni^{4+} couples, which is close to the rational value in Cr-doped $LiNi_{0.5}Mn_{1.5}O_4$ [13]. According to the capacity contribution by Mn^{3+}/Mn^{4+}, the oxygen deficiency δ in $LiNi_{0.5}Mn_{1.5}O_{4-\delta}$ is estimated to be 0.02. Fig. 2b presents CV plots of $LiNi_{0.5}Mn_{1.5}O_4$ at

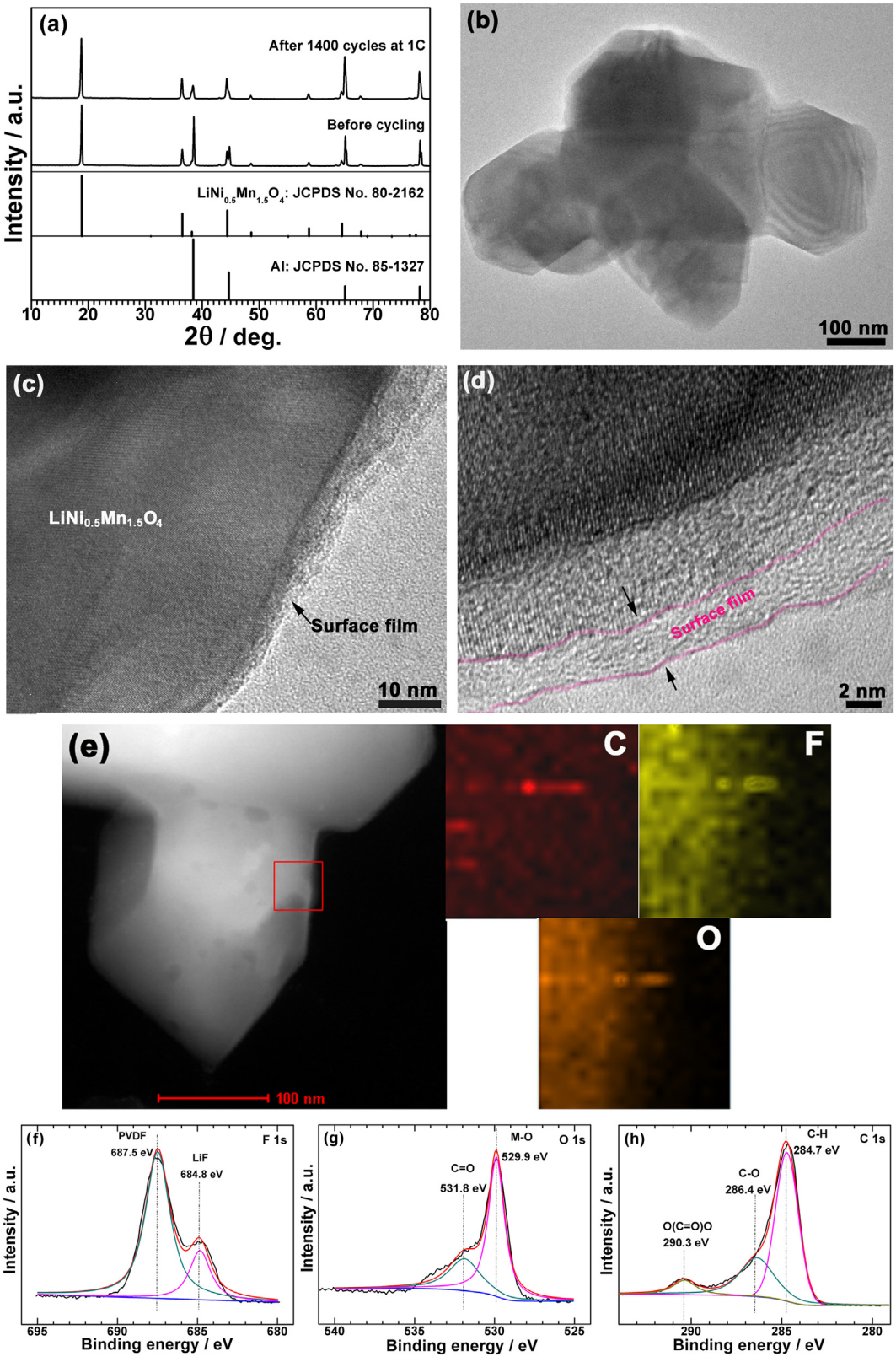

Fig. 4. (a) XRD patterns, (b–d) TEM images, (e) EDS mapping, and (f–h) XPS of the cycled $LiNi_{0.5}Mn_{1.5}O_4$ sample.

0.1 mV s^{-1}, where the current peaks at around 4.0 V correspond to Mn^{3+}/Mn^{4+} couple, while the two successive peaks at 4.5–4.9 V are assigned to Ni^{2+}/Ni^{3+} and Ni^{3+}/Ni^{4+} couples. Note that the two peaks of Ni^{2+}/Ni^{3+} and Ni^{3+}/Ni^{4+} are well separated and become sharp after the first cycle, indicating good electrode kinetics of $LiNi_{0.5}Mn_{1.5}O_4$ with a submicron size.

Fig. 2c shows the voltage profiles of $LiNi_{0.5}Mn_{1.5}O_4$ on 100–800 cycles at 1 C. The submicron $LiNi_{0.5}Mn_{1.5}O_4$ exhibits slow capacity fade from 122 mAh g^{-1} at the 100th cycle to 114 mAh g^{-1} at the 400th cycle, corresponding to capacity retention of 93%. In addition, the curves resemble one another with well defined, separated potential plateaus, indicative of good preservation of perfect crystallographic ordering of $LiNi_{0.5}Mn_{1.5}O_4$ during cycling which has been verified by XRD (Fig. 4a) and TEM (Fig. 4b and c) of the cycled sample. Of note is that even after 800 cycles, the shape and length of the 4.0 V plateau are almost unchanged, suggesting that the Mn^{3+} ions can survive repeated cycling at a high rate. In other words, the disproportionation reaction $2Mn^{3+} = Mn^{2+} + Mn^{4+}$ that leads to the dissolution of Mn^{2+} [16] is not significant due probably to the protective effect of the surface film. As suggested by Xiao et al. [13], an appropriate Mn^{3+} concentration will minimize the potential generation of the soluble Mn^{2+} ions via the disproportionation reaction. In contrast, the length of the 4.7 V plateaus is on the decrease during long-term cycling which suggests that the inhibition effect for Ni dissolution is less effective. Fig. 2d demonstrates CV plots during 100–800 scans at 0.1 mV s^{-1}. The almost overlapped current peaks at 4.0 V also indicate the durability of Mn^{3+}/Mn^{4+} redox couple, while the broadening and intensity decrease of the current peaks at 4.7 V signify the degraded kinetics of Ni^{2+}/Ni^{4+} redox couple.

Rate performance is one of the important factors for the practical application of $LiNi_{0.5}Mn_{1.5}O_4$ in EVs and HEVs. Rate capability of the submicron $LiNi_{0.5}Mn_{1.5}O_4$ is investigated as illustrated in Fig. 2e and f. As seen in Fig. 2e, the discharge plateaus at both 4.0 V and 4.7 V are well defined and separated up to 1 C rate. At higher rates, high discharge plateaus (above 4.5 V) related to Ni^{2+}/Ni^{4+} are still observable although the separation of the plateaus becomes unclear with increased rate. In addition, the 4 V plateau related to Mn^{3+}/Mn^{4+} still exists at 5 C, indicating high kinetics of Mn^{3+}/Mn^{4+} redox couple, possibly due to the small size of $LiNi_{0.5}Mn_{1.5}O_4$. Fig. 2f gives the rate dependence of the discharge capacity of $LiNi_{0.5}Mn_{1.5}O_4$. The discharge capacities (the last cycle at each rate) of $LiNi_{0.5}Mn_{1.5}O_4$ at 0.1, 0.2, 0.5, 1, 5, 10, 20 C are 122.3, 121.6, 119.6, 118.8, 115.1, 113.3, and 105.8 mAh g^{-1}, respectively. Note that the discharge capacity is almost independent of the applied current density at 0.1–1 C rates. At 1 C, a high discharge capacity of 118.8 mAh g^{-1} can be obtained for $LiNi_{0.5}Mn_{1.5}O_4$. Even at 20 C, it can still yield a discharge capacity of 105.8 mAh g^{-1}, indicative of its excellent rate capability. When the current is shifted to 0.1 C, the discharge capacity can be recovered to 115.5 mAh g^{-1}, suggesting that the crystallographic ordering of $LiNi_{0.5}Mn_{1.5}O_4$ can be preserved after high-rate cycling. The good rate capability of $LiNi_{0.5}Mn_{1.5}O_4$ can be attributed mainly to two factors: (1) the submicron structure facilitates the Li ions transport both at particle/electrolyte interface and in bulk particles and (2) Mn^{3+} formation can contribute to both Li ions diffusion rate by promoting Mn–Ni site disorder [13] and electronic conductivity by electron hopping between Mn^{3+} and Mn^{4+} [12].

Besides rate performance, cycling stability is another critical factor for the practical application of $LiNi_{0.5}Mn_{1.5}O_4$ in EVs and HEVs. After 1400 cycles at 1 C, a discharge capacity of around 80.0 mAh g^{-1} still yieldable for $LiNi_{0.5}Mn_{1.5}O_4$ (Fig. 2g), which indicates long-term cycling stability of $LiNi_{0.5}Mn_{1.5}O_4$. In addition, the coulombic efficiency is close to 100% after the first three cycles at 0.1 C and one cycle at 1 C, indicative of good reversibility of $LiNi_{0.5}Mn_{1.5}O_4$. As shown in Fig. 2h, $LiNi_{0.5}Mn_{1.5}O_4$ can deliver a discharge capacity of around 80 mAh g^{-1} after 500 cycles at 5 C. Stable cycling is also observed at low rates as seen in Fig. 2i. The excellent high-rate cycling stability is due mainly to the durability of Mn^{3+} ions in $LiNi_{0.5}Mn_{1.5}O_4$ lattice to ensure high-rate cycling and the protective effect of the surface film to reduce the Ni and Mn dissolution by HF. TEM and XPS characterizations on the cycled sample were performed to reveal the structure and composition of the surface film. TEM image in Fig. 4c and d shows the presence of a layer of film of 2–3 nm thickness on the surface of a cycled $LiNi_{0.5}Mn_{1.5}O_4$ particle and the surface film contains C, F and O elements confirmed by EDS mapping (Fig. 4e). To further check the composition of the surface film, XPS characterization was conducted on the cycled sample as seen in Fig. 4f–h. The results confirm that the main compositions of the surface film are LiF and Li_2CO_3 [28,31–33]. The work by Yang et al. [33] showed that the in-situ generated amorphous Li_2CO_3 layer could suppress the interfacial side reaction between the active material and the $LiPF_6$-contained electrolyte. It should be noted that long-term cycling also leads to capacity fade of $LiNi_{0.5}Mn_{1.5}O_4$. Nevertheless, this work provides a facile method to obtain high-performance $LiNi_{0.5}Mn_{1.5}O_4$ with controlled particle size and rational Mn^{3+} concentration. Table 1 summarizes the rate and cycling performance of previously reported $LiNi_{0.5}Mn_{1.5}O_4$ samples and those of our $LiNi_{0.5}Mn_{1.5}O_4$ sample. These $LiNi_{0.5}Mn_{1.5}O_4$ samples represent the best ones reported so far. From these data we can see that the electrochemical performance of our sample, prepared by a simple solid-phase route, is among the best ones.

Full cells $LiNi_{0.5}Mn_{1.5}O_4$–MCMB were fabricated to further investigate the practical application of $LiNi_{0.5}Mn_{1.5}O_4$. The MCMB anodes composed of 75 wt% MCMB, 15 wt% AB and 10 wt% PVDF were prepared by a same route as the $LiNi_{0.5}Mn_{1.5}O_4$ cathodes. The first irreversible capacity of MCMB was reduced by soaking the electrodes in $LiPF_6$/EC + DMC electrolyte for 90 min before the full cells assembly. The full cells are cathode limited by controlling the $LiNi_{0.5}Mn_{1.5}O_4$/MCMB weight ratio at around 2:3. Fig. 3a shows the first three voltage profiles of $LiNi_{0.5}Mn_{1.5}O_4$–MCMB cell

Table 1
Summary of rate and cycling performance of $LiNi_{0.5}Mn_{1.5}O_4$.

Sample	Preparation method	Rate capability (mAh g^{-1})			Capacity retention	Reference
		1 C	10 C	20 C		
$LiNi_{0.5}Mn_{1.5}O_4$	Solid phase firing	118.8	113.3	105.8	62.2% after 1400 cycles at 1 C	This work
$LiNi_{0.45}Cr_{0.05}Mn_{1.5}O_4$	Solid phase firing	120.0	100.0	–	99.6% after 250 cycles at 1 C	[13]
$LiNi_{0.5}Mn_{1.5}O_4$	Sol–gel route/solid phase firing	125.0	112.5	96.0	89.0% after 500 cycles at 1 C	[24]
$LiNi_{0.5}Mn_{1.5}O_4$	Template route/solid phase firing	133.3	123.0	115	86.0% after 500 cycles at 1 C	[25]
$LiNi_{0.5}Mn_{1.5}O_4$	Solution route/solid phase firing	140.0	120.0	109.0	91.0% after 500 cycles at 5 C	[28]
$LiNi_{0.5}Mn_{1.5}O_4$	Impregnation/solid phase firing	118.0	111.5	104.0	97.6% after 200 cycles at 1 C	[29]
$LiNi_{0.4}Ru_{0.05}Mn_{1.5}O_4$	Solid phase firing	130.0	117.0	–	84.0% after 500 cycles at 10 C	[34]
$LiNi_{0.5}Mn_{1.5}O_4$	Solution route/solid phase firing	–	112.1	–	76.0% after 1500 cycles at 2 C	[35]
$LiNi_{0.5}Mn_{1.5}O_4$/graphene oxide	Solution route/solid phase firing	<110.0	<70.0	–	61.0% after 1000 cycles at 1/2 C	[36]

at 0.1 C. The cell can yield a first discharge capacity of 125.5 mAh g^{-1}, close to the value in the half cells. In addition, the full cell exhibits a high working voltage of around 4.5 V. This means that a high energy density can be achieved for $LiNi_{0.5}Mn_{1.5}O_4$–MCMB cell considering its high capacity and voltage. As shown in Fig. 3b, a first discharge capacity of 118.0 mAh g^{-1} is obtained at 1 C, which is also close to the value in the half cells. After 120 cycles at 1 C, a discharge capacity of 90.0 mAh g^{-1} is still obtainable. $LiNi_{0.5}Mn_{1.5}O_4$ is also an ideal cathode to couple with high-voltage anodes, for instance $Li_4Ti_5O_{12}$ [37,38], considering its high working voltage of 4.7 V.

4. Conclusions

In summary, submicron $LiNi_{0.5}Mn_{1.5}O_4$ ($Fd\bar{3}m$) has been synthesized by a facile solid-phase method at 800 °C. The submicron $LiNi_{0.5}Mn_{1.5}O_4$ shows excellent electrochemical performance in both $LiNi_{0.5}Mn_{1.5}O_4$–Li half cells and $LiNi_{0.5}Mn_{1.5}O_4$–MCMB full cells. The results revealed that Mn^{3+} at a rational concentration in $LiNi_{0.5}Mn_{1.5}O_4$ lattice exhibits high-rate durability upon repeated cycling. Both small size and presence of Mn^{3+} contribute to excellent rate performance of $LiNi_{0.5}Mn_{1.5}O_4$, where a high discharge capacity of 105.8 mAh g^{-1} at 20 C is obtainable for half cells. The high-rate durability of Mn^{3+}, together with the small size induced effective protective film, promotes long-term cycling stability of $LiNi_{0.5}Mn_{1.5}O_4$ at high rates. The half cell can retain a discharge capacity of around 80 mAh g^{-1} after 1400 cycles at 1 C, and the full cell can deliver a discharge capacity of 90.0 mAh g^{-1} after 120 cycles at 1 C. The excellent electrochemical performance and easy synthesis of the submicron $LiNi_{0.5}Mn_{1.5}O_4$ make it a promising cathode for high-energy-density Li-ion batteries.

Acknowledgments

This work was supported by National Basic Research Program of China (2013CB934001), the National Natural Science Foundation of China (No. 51101139), Key Science and Technology Innovation Team of Zhejiang Province under Grant Number 2010R50013, and Program for Innovative Research Team in University of Ministry of Education of China (IRT13037).

References

[1] J.B. Goodenough, Y. Kim, Chem. Mater. 22 (2010) 587–603.
[2] B.L. Ellis, K.T. Lee, L.F. Nazar, Chem. Mater. 22 (2010) 691–714.
[3] V. Etacheri, R. Marom, R. Elazari, G. Salitra, D. Aurbach, Energy Environ. Sci. 4 (2011) 3243–3262.
[4] B. Xu, D.N. Qian, Z.Y. Wang, Y.S. Meng, Mater. Sci. Eng. R 73 (2012) 51–65.
[5] O.K. Park, Y. Cho, S. Lee, H.C. Yoo, H.K. Song, J. Cho, Energy Environ. Sci. 4 (2011) 1621–1633.
[6] A. Kraytsberg, Y. Ein Eli, Adv. Energy Mater. 2 (2012) 922–939.
[7] R. Santhanam, B. Rambabu, J. Power Sources 195 (2010) 5442–5451.
[8] M. Hu, X.L. Pang, Z. Zhou, J. Power Sources 237 (2013) 229–242.
[9] Q. Zhong, A. Bonakdarpour, M. Zhang, Y. Gao, J.R. Dahn, J. Electrochem. Soc. 144 (1997) 205–213.
[10] Y. Terada, K. Yasaka, F. Nishikawa, T. Konishi, M. Yoshio, I. Nakai, J. Solid State Chem. 156 (2001) 286–291.
[11] J.H. Kim, S.T. Myung, C.S. Yoon, S.G. Kang, Y.K. Sun, Chem. Mater. 16 (2004) 906–914.
[12] M. Kunduraci, J.F. Al Sharab, G.G. Amatucci, Chem. Mater. 18 (2006) 3585–3592.
[13] J. Xiao, X. Chen, P.V. Sushko, M.L. Sushko, L. Kovarik, J. Feng, Z. Deng, J. Zheng, G.L. Graff, Z. Nie, D. Choi, J. Liu, J.G. Zhang, M.S. Whittingham, Adv. Mater. 24 (2012) 2109–2116.
[14] J. Cabana, M. Casas Cabanas, F.O. Omenya, N.A. Chernova, D.L. Zeng, M.S. Whittingham, C.P. Grey, Chem. Mater. 24 (2012) 2952–2964.
[15] D.W. Shin, C.A. Bridges, A. Huq, M.P. Paranthaman, A. Manthiram, Chem. Mater. 24 (2012) 3720–3731.
[16] J. Song, D.W. Shin, Y.H. Lu, C.D. Amos, A. Manthiram, J.B. Goodenough, Chem. Mater. 24 (2012) 3101–3109.
[17] G.Q. Liu, K.S. Park, J. Song, J.B. Goodenough, J. Power Sources 243 (2013) 260–266.
[18] W. Zhu, D. Liu, J. Trottier, C. Gagnon, A. Mauger, C.M. Julien, K. Zaghib, J. Power Sources 242 (2013) 236–243.
[19] H. Kawaura, D. Takamatsu, S. Mori, Y. Orikasa, H. Sugaya, H. Murayama, K. Nakanishi, H. Tanida, Y. Koyama, H. Arai, Y. Uchimoto, Z. Ogumi, J. Power Sources 245 (2014) 816–821.
[20] H. Konishi, K. Suzuki, S. Taminato, K. Kim, S. Kim, J. Lim, M. Hirayama, R. Kanno, J. Power Sources 246 (2014) 365–370.
[21] Y.S. Lee, Y.K. Sun, S. Ota, T. Miyashita, M. Yoshio, Electrochem. Commun. 4 (2002) 989–994.
[22] M.G. Lazarraga, L. Pascual, H. Gadjov, D. Kovacheva, K. Petrov, J.M. Amarilla, R.M. Rojas, M.A. Martin Luengo, J.M. Rojo, J. Mater. Chem. 14 (2004) 1640–1647.
[23] K.M. Shaju, P.G. Bruce, Dalton Trans. (2008) 5471–5475.
[24] H.B. Lin, Y.M. Zhang, J.N. Hu, Y.T. Wang, L.D. Xing, M.Q. Xu, X.P. Li, W.S. Li, J. Power Sources 257 (2014) 37–44.
[25] Z.X. Chen, S. Qiu, Y.L. Cao, X.P. Ai, K. Xie, X.B. Hong, H.X. Yang, J. Mater. Chem. 22 (2012) 17768–17772.
[26] H.W. Lee, P. Muralidharan, C.M. Mari, R. Ruffo, D.K. Kim, J. Power Sources 196 (2011) 10712–10716.
[27] E. Hosono, T. Saito, J. Hoshino, Y. Mizuno, M. Okubo, D. Asakura, K. Kagesawa, D. Nishio Hamane, T. Kudo, H.S. Zhou, CrystEngComm 15 (2013) 2592–2597.
[28] X.L. Zhang, F.Y. Cheng, J.G. Yang, J. Chen, Nano Lett. 13 (2013) 2822–2825.
[29] L. Zhou, D.Y. Zhao, X.W. Lou, Angew. Chem. Int. Ed. 51 (2012) 239–241.
[30] M. Kunduraciz, G.G. Amatucci, J. Electrochem. Soc. 153 (2006) A1345–A1352.
[31] J. Liu, A. Manthiram, Chem. Mater. 21 (2009) 1695–1707.
[32] M.Y. Nie, D.P. Abraham, Y.J. Chen, A. Bose, B.L. Lucht, J. Phys. Chem. C 117 (2013) 13403–13412.
[33] S.F. Yang, J. Chen, Y.J. Liu, B.L. Yi, J. Mater. Chem. A (2014), http://dx.doi.org/10.1039/C4TA01147C.
[34] H.L. Wang, H. Xia, M.O. Lai, L. Lu, Electrochem. Commun. 11 (2009) 1539–1542.
[35] Y.X. Qian, Y.F. Deng, Z.C. Shi, Y.B. Zhou, Q.C. Zhuang, G.H. Chen, Electrochem. Commun. 27 (2013) 92–95.
[36] X. Fang, M.Y. Ge, J.P. Rong, C.W. Zhou, J. Mater. Chem. A 1 (2013) 4083–4088.
[37] Y.L. Ding, B.M. Goh, H. Zhang, K.P. Loh, L. Lu, J. Power Sources 236 (2013) 1–9.
[38] W.K. Pang, N. Sharma, V.K. Peterson, J.J. Shiu, S.H. Wu, J. Power Sources 246 (2014) 464–472.